Physics of the Earth and Planetary Interiors 184 (2011) 194–207

Contents lists available at ScienceDirect

Physics of the Earth and Planetary Interiors

journal homepage: www.elsevier.com/locate/pepi

Coast effect distortion of marine magnetotelluric data: Insights from a pilot study offshore northeastern Japan

Kerry Key*, Steven Constable

Scripps Institution of Oceanography, University of California San Diego, 9500 Gilman Drive, La Jolla, CA 92093-0225, USA

ARTICLE INFO

Article history:
Received 11 September 2010
Received in revised form
11 November 2010
Accepted 17 November 2010

Edited by: Kei Hirose.

Keywords:
Magnetotelluric
Marine electromagnetics
Electrical properties
Subduction zones

ABSTRACT

We report on strong coast effect distortions observed for broadband marine magnetotelluric (MT) data collected on the forearc offshore northeastern Japan. Eight days of horizontal electric and magnetic fields recorded at eight seafloor stations and the horizontal magnetic fields from a land remote station were processed with a robust multiple-station algorithm, yielding good MT responses and inter-station transfer functions at periods of 7–10,000 s. Transverse electric (TE) mode responses have cusps in apparent resistivity and negative phases at periods around 1000 s, while the transverse magnetic (TM) mode responses are galvanically depressed below the TE responses. An analysis of inter-station transfer functions confirms that the apparent resistivity cusps are a magnetic field, rather than electric field, phenomenon, consisting of an amplitude minimum and rapid phase change around a characteristic frequency. Poynting vectors for a TE coast effect model study illustrate that the anomalous phases are associated with energy diffusing back up to the seafloor from below, after being turned around from its usual downward propagating trajectory by inductive coupling between the conductive ocean and the resistive seafloor along the continental margin. We show that the characteristic frequency and position of the TE mode apparent resistivity cusps are determined by a relatively simple combination of the electrical resistivity of the seafloor, the depth of the ocean, and the distance from the coastline. By including coastlines and bathymetry in 2D inversion, we recover the seafloor conductivity structure along the forearc, demonstrating that broadband data can constrain the thickness of conductive forearc sediments and the underlying high resistivity associated with the mantle wedge and subducting oceanic lithosphere.

1. Introduction

In this paper we examine the nature of the ocean-side coast effect and its influence on marine magnetotelluric (MT) data. The geomagnetic coast effect was first observed as a land-side phenomenon consisting of a steepening of normally horizontal magnetic field fluctuations at periods of several thousand seconds near the coast in Australia (Parkinson, 1959) and Japan (Rikitake, 1959). Parkinson (1962) correctly inferred that this was a consequence of induction in the oceans, and efforts to model the coast effect drove the first two-dimensional (2D) numerical models of geomagnetic induction (Jones and Price, 1970). It was also recognized early on that the land-side coast effect may depend not only on induction in the ocean, but also on conductivity contrasts in the deeper (mantle) structure between continent and ocean, and numerous efforts were made to interpret the available data in terms of such structure. Parkinson and Jones (1979) provide a comprehensive early review of this work. The land-side coast effect is exemplified by the ratio of the vertical to horizontal magnetic fields at a particular frequency, or (equivalently), the size of induction vectors (or tipper, in MT parlance), which point towards the ocean near coastlines. In a 2D context, the land-side coast effect is a TE-mode phenomenon (called E-polarization in the older literature), in which the MT component has an electric field parallel to strike (or the coastline, in this case). Taking a simplistic view, a coast-parallel current sheet induced in the ocean produces a vertical magnetic field at its edge, which accounts for the steepening of the observed fields.

In contrast to the land-side coast effect, the ocean-side coast effect has traditionally been considered to be a TM-mode (or H-polarization) phenomenon, in which low frequency electric fields perpendicular to the coast are attenuated as a consequence of current being interrupted by the more resistive continental rocks (Cox, 1980). Since the MT apparent resistivity is derived from the ratio of electric to magnetic fields, this behavior has the effect of suppressing the resistivity of the coast-perpendicular mode. In a provocative paper, Heinson and Constable (1992) suggested that this suppression of apparent resistivities extended to three dimensions and

* Corresponding author. Tel.: +1 858 822 2975.
E-mail addresses: kkey@ucsd.edu (K. Key), sconstable@ucsd.edu (S. Constable).
URLs: http://marineemlab.ucsd.edu/kkey (K. Key), http://marineemlab.ucsd.edu/steve (S. Constable).

0031-9201/$ – see front matter © 2010 Elsevier B.V. All rights reserved.
doi:10.1016/j.pepi.2010.11.008

was ubiquitous throughout the ocean basins. They suggested that apparent resistivities depressed in all directions were responsible for unrealistically high mantle conductivities being inferred from 1D interpretations of long-period marine MT data. Although controversial at the time (Tarits et al., 1993; Constable and Heinson, 1993), it is now generally recognized that the effects of bathymetry and the coastlines need to be incorporated into marine MT interpretation (e.g., White et al., 1997; Baba and Chave, 2005; Seama et al., 2007; Matsuno et al., 2010).

Returning to the land-side coast effect, it is interesting to note that early efforts to model the contribution of oceanic/continental mantle conductivity contrasts as part of the TE-mode coast effect often used marine MT interpretations that were overly conductive as a result of TM-mode distortions (e.g., Parkinson and Jones, 1979; Menvielle et al., 1982), or inferred a highly conductive oceanic mantle based on a purely 2D interpretation of long-period marine MT data which may have been subjected to 3D TM-mode type distortion (e.g., Kellett et al., 1991). It should be emphasized that much of this early work was based on long-period MT data where the shortest period recorded was 1000 s or longer, skin depths in seawater were greater than the ocean depth (allowing thin-sheet modeling), and the compensation distance, defined by Cox (1980) as the e-folding distance over which the TM-mode coast effect operated, is thousands of kilometers.

Largely spurred by interest in economic exploitation of the continental shelves, marine MT studies have recently focussed on acquiring much shorter period data (down to 1 s or so, depending on water depth and signal strength) by using sensors and sampling rates optimized for higher frequencies, typically induction coil magnetometers and high-gain AC-coupled electric field sensors (e.g., Constable et al., 1998). This so-called broadband instrumentation covers a bandwidth of about 1–10,000 s, whereas traditional long period marine MT instrumentation operates at about 500–100,000 s. This has allowed the collection of MT data with increased sensitivity to crustal structure and that is inductively decoupled from the TM coast effect when far from the nearest land (e.g., Key and Constable, 2002). However, when data are collected close to coastlines, not only is the classic TM-mode depression of apparent resistivities observed, but the TE-mode coast effect is manifest as peaks (or cusps) in apparent resistivity and negative phases.

Ferguson (1988) is probably the first to report a seafloor TE mode coast effect, noting unusual TE phases and apparent resistivity cusps at about 1000 s in long period data collected in the Tasman sea, and documenting that these effects arise from magnetic field distortion resulting from the nearby Australian and New Zealand coastlines. Constable et al. (2009) reported negative TE phases and apparent resistivity cusps at 100 s period in the San Diego Trough, offshore California, and explained it in terms of the same steepening of the magnetic field as is observed in the land-side coast effect. Alekseev et al. (2009) presented a brief model study showing that the anomalous TE phase is predominantly due to large magnetic field phase, rather than the electric phase. Here we report even more extreme behavior in some early broadband marine MT data collected offshore Japan, localized at a period of around 1000 s. We show that the frequency and position of the TE mode apparent resistivity cusps are determined by a relatively simple combination of the electrical resistivity of the seafloor, the depth of the ocean, and the distance from the coastline. An analysis of inter-station transfer functions demonstrates how the apparent resistivity cusps are a magnetic field, rather than electric field, phenomenon. Examination of the Poynting vector shows that negative TE phases are associated with energy diffusing back up to the seafloor from below after being turned around from its usual downward propagating trajectory by inductive coupling with the coastline topography.

Although the purpose of the current paper is to develop a deeper physical understanding of the ocean-side coast effect, we show that by including coastlines and bathymetry in 2D inversion one can recover seafloor conductivity structure, as demonstrated by Constable et al. (2009). Three dimensional bathymetry and coastlines, however, present a severe challenge to current numerical capabilities, since it is clear that the near-shore coast effect is strongly coupled to seafloor conductivity structure.

2. Broadband marine MT survey

In May 2000 we carried out deployments of a newly developed broadband marine MT instrument on the accretionary prism of the Japan trench as a pilot study to examine the use of MT sounding to characterize the seismogenic zone; preliminary results were presented in Mikada et al. (2000). The survey region lies on the forearc of the Japan trench where the Pacific plate is subducted beneath the northeastern Japan island arc at 8 cm/year. Earthquakes occur near the top of the subducting plate over a distance of at least 300 km, spanning from the outer rise to beneath the island of Honshu; the area has been subjected to several strong earthquakes of M7 and greater, including the M_w 8.4 great Sanriku earthquake of 1933 and the 1968 Tokachi-Oki M_w 8.2 earthquake (e.g., Gamage et al., 2009; Hino et al., 2009). Seismic surveys, using both seismic reflection profiling and ocean-bottom seismometers, have been carried out to characterize the forearc sediments and mantle wedge, the subducting plate, and earthquakes (Ito et al., 2000, 2004; Hino et al., 2000; Tsuru et al., 2000; Hayakawa et al., 2002; Fujie et al., 2006; Itoh and Tsuru, 2006). The role of the MT method is to characterize the quantity and distribution of fluids in the accretionary prism and subducting slab, since porosity, pore pressure and subducting fluids have a large influence on earthquake generation.

Because of the MT method's inherent sensitivity to increased electrical conductivity associated with water and partial melt, it has been used fairly extensively to study subduction systems, mainly using data acquired on land. The earliest example is the Vancouver Island study of Kurtz et al. (1986). More recently studies have been carried out in New Zealand (Wannamaker et al., 2009), South America (Schwarz and Krüger, 1997; Brasse and Eydam, 2008; Booker et al., 2004), and Mexico (Jödicke et al., 2006). Examples of marine MT data being used to study subduction zones includes the amphibious EMSLAB experiment (Wannamaker et al., 1989) and the purely marine MT study of the Mariana subduction zone (Matsuno et al., 2010), both of which used long period instrumentation, resulting in a response bandwidth of 1000–100,000 s period.

We deployed 10 seafloor MT instruments on a line 100–200 km offshore and perpendicular to the coast of Honshu, about 100 km south of the junction with the Kuril trench. The geology and bathymetry are locally 2D but become 3D towards the north where Honshu and the Japan trench join the Kuril trench, Hokkaido, and the Kuril Islands (Fig. 1). The instruments were deployed for 11–13 days in water depths from 1200 to 5400 m, and all were recovered with data and one with an octopus. Eight of the instruments were the then recently developed 16-bit instruments described by Constable et al. (1998), sampling at 25 Hz and equipped with commercial induction coil magnetometers (model BF-4 manufactured by EMI) and high-gain AC-coupled electric field amplifiers connected to silver chloride electrodes on 10 m orthogonal dipoles. Two instruments (sites 3 and 10) were prototypes using 24-bit digitization sampling at 125 Hz. However, an adverse interaction between the magnetometer coils and the electric field amplifiers on these instruments compromised the data quality; we do not include these in the analysis presented here.

All instruments recorded 4 channels of data from two horizontal magnetometer coils and two horizontal electric field antenna

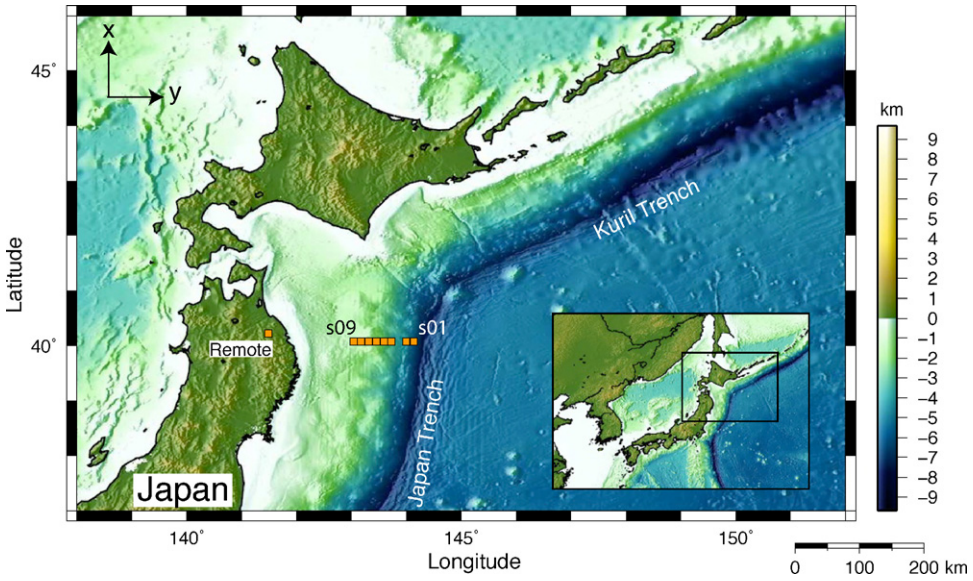

Fig. 1. Topographic map showing the location of the seafloor magnetotelluric survey offshore Northeastern Japan. Orange squares show the location of the eight seafloor MT stations and the Iwate district onshore remote site. Arrows in the upper left corner denote the coordinate axes used for the MT responses.

onto a 2 Gbyte hard drive, under control of an Onset Tattletale 8 microcontroller. Timing was provided by onboard clocks set before deployment using GPS time and checked against GPS time on recovery; time drift was typically 20 ms over the experiment, corresponding to less than one degree phase error at the shortest periods. Orientations were recorded using a mechanical compass which was locked after deployment by a clamping mechanism and a timer based on dissolving sugar crystals, and checked by comparison of transfer functions with a land site. Magnetometers and land versions of the logging equipment were installed in the Iwate and Ashiro districts on Honshu, to provide remote references. We have since determined that land-based remote references are not required for marine MT processing, but in this case it provided the opportunity to compute transfer functions between the land and marine magnetic fields. A representative 60 min section of the time series from a few stations is shown in Fig. 2.

This was one of the first deep-water deployments of an MT receiver capable of recording much shorter period signal than possible with conventional long period marine MT sensors (e.g., Filloux, 1973). While we have modified and improved the instrument over the intervening decade in many ways (8 channels of 24 bit recording, custom microcontroller, storage on compact flash, external electronic recording compasses, custom low-power lightweight magnetometer coils, and broader bandwidth electric field amplifiers), the instrument used in the project described here is functionally the same as the current broadband MT instrument, capable of recording high quality MT data at full ocean depths in the period range 10–10,000 s. One critical aspect of the MT receiver that has not changed over its development history is the careful coupling of the instrument frame to a 100–200 kg concrete anchor slab in order to minimize motional noise on the magnetometers. Conventional long-period instruments, typically using fluxgate magnetometers and smaller anchor systems, collect data down to periods of several hundred seconds at best, and extend the long-period range to about 100,000 s at the cost of significantly extended deployment time (typically at least a few months), requiring separate deployment and recovery cruises. In contrast, the broadband system can obtain reliable MT responses at shorter periods with deployments lasting only a few days to weeks during a single cruise (e.g., Key and Constable, 2002; Key et al., 2006; Constable et al., 2009).

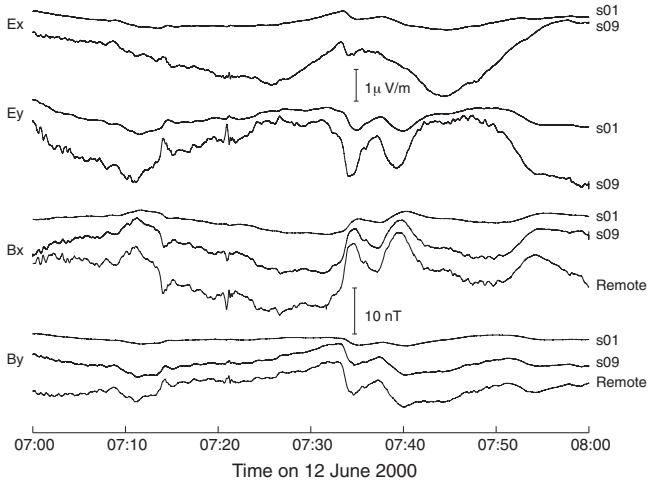

Fig. 2. Sixty minutes of magnetotelluric data recorded at the land remote site and seafloor stations s09 (1200 m water) and s01 (5400 m water). The relative lack of high frequency variations for s01 results from the increased source field attenuation due to its deeper water depth. Each channel has been correct for the frequency dependent sensor response and then rotated to x = north and y = east.

3. Array transfer function estimation

MT responses were computed using a robust multiple-station response estimation procedure (Egbert, 1997). This method analyzes all data channels in an array of stations in order to robustly identify coherent magnetotelluric signal from incoherent noise. This approach conveniently allows for the estimation of transfer functions between any pairs of channels in the entire array. For example, the transfer tensor relationships between the fields at stations i and j can be written for magnetic fields $\mathbf{H}$ and electric fields $\mathbf{E}$ as

$$\mathbf{H}_i = \mathbf{M}_{i,j}\mathbf{H}_j, \tag{1}$$

$$\mathbf{E}_i = \mathbf{T}_{i,j}\mathbf{E}_j, \tag{2}$$

$$\mathbf{E}_i = \mathbf{Z}_{i,j}\mathbf{H}_j, \tag{3}$$

where $\mathbf{Z}_{i,i}$ is the standard MT impedance tensor relationship for electric and magnetic fields at station i and $\mathbf{Z}_{i,j}$ represents hybrid impedances for electric and magnetic fields recorded at different stations. These tensors expand into 2×2 matrices. For example:

$$\mathbf{Z} = \begin{pmatrix} Z_{xx} & Z_{xy} \\ Z_{yx} & Z_{yy} \end{pmatrix}. \quad (4)$$

The utility of these transfer tensors can be elucidated by noting that the magnetotelluric source field $\mathbf{H}_0$ and the observable magnetic and electric fields $\mathbf{H}$ and $\mathbf{E}$, which are a combination of the external source field and internally induced fields, can be compactly represented using transfer tensors (e.g., Berdichevsky and Zhdanov, 1984):

$$\begin{aligned} \mathbf{H}_i &= \mathbf{P}_{i,0}\mathbf{H}_0, \\ \mathbf{E}_i &= \mathbf{Q}_{i,0}\mathbf{H}_0, \end{aligned} \quad (5)$$

where $\mathbf{P}$ and $\mathbf{Q}$ are transfer tensors that contain the fundamental information on the source field interaction with Earth structure. Since Earth's conductivity generates induced fields everywhere, it is not feasible to measure $\mathbf{H}_0$ directly. Instead, cancellation of $\mathbf{H}_0$ in the expressions above results in:

$$\mathbf{M}_{i,j} = \mathbf{P}_{i,0}\mathbf{P}_{j,0}^{-1}, \quad (6)$$

$$\mathbf{T}_{i,j} = \mathbf{Q}_{i,0}\mathbf{Q}_{j,0}^{-1}, \quad (7)$$

$$\mathbf{Z}_{i,j} = \mathbf{Q}_{i,0}\mathbf{P}_{j,0}^{-1}. \quad (8)$$

These expressions show that the measurable tensors $\mathbf{M}$, $\mathbf{T}$ and $\mathbf{Z}$ are linear combinations of the fundamental Earth responses $\mathbf{P}$ and $\mathbf{Q}$. Since the impedance tensor $\mathbf{Z}$ contains both $\mathbf{P}$ and $\mathbf{Q}$ terms, it effectively captures the magnetotelluric response of the Earth, whereas $\mathbf{M}$ and $\mathbf{T}$ separately describe aspects of the response that are unique to magnetic and electric field variations across the array, and may allow for further constraints on conductivity structure (e.g., Egbert, 2002; Berdichevsky and Dmitriev, 2008). A more complete discussion of the full response space of geomagnetic induction data can be found elsewhere (Egbert and Booker, 1989; Egbert, 1997).

For the array processing of our data set, eight days of simultaneous time-series from the eight seafloor stations and the onshore remote magnetic station were divided up into 128 point sections with 32 points of overlap using a cascade-decimation procedure that maximizes the number of independent samples available for statistical response estimation (Wight and Bostick, 1980). Each section was pre-whitened with a four-term autoregressive sequence, windowed with a Hamming taper, Fourier transformed and then corrected for filter responses, gains and the pre-whitening. The Fourier coefficients from all channels were then processed in a robust multivariate errors-in-variables algorithm that estimates response eigenvectors for the entire array, from which the tensors $\mathbf{M}$, $\mathbf{T}$ and $\mathbf{Z}$ were then computed (Egbert, 1997). This method obtained good quality responses at periods of about 7–5000 s, where the short period limit is governed by severe attenuation of the high frequencies through the conductive seawater and the long period limit is due to the relatively short recording time.

4. Impedance responses

The resulting MT apparent resistivity and phase responses are shown in Fig. 3. The strong increase in the apparent resistivity is indicative of near surface conductive sediments underlain by a resistive basement. The responses also show characteristics we have previously observed in seafloor MT data that have been distorted by seafloor topography and the coastline near the San Diego Trough (Constable et al., 2009). The identifying characteristics of such distortions are cusps in the TE mode apparent resistivity, negative TE phases and a galvanic depression of the TM mode apparent resistivity. The responses show a systematic increase in these distortions with site location, with the largest negative phases and cusps in the Z_{xy} (TE) data for the three deepest stations (s04, s02 and s01). While the general character of the distortions is similar to those observed in the San Diego Trough, their magnitude is much different for this data set. For the Trough data, the negative TE phases and the TE mode apparent resistivity cusps are centered around a period of about 200 s, with the most negative phase reaching to -15°. The deepest sites in this project have a TE mode cusp centered around a longer period of about 1600 s, while the most negative phase is observed at site s01, where it reaches -65° at 1600 s period. Two stations, s01 and s04, also exhibit negative phases for the shortest period Z_{yx} (TM) data. For the deepest sites, the TE phase at long periods rapidly increases from large negative to large positive values over periods of 1000–3000 s. Unlike the Trough data, which have depressed TM mode apparent resistivities that are up to a factor of 500 times smaller than the TE mode, the data here show a smaller TM mode depression by a factor of 10 at periods greater than 500 s and a factor of 3 or less at the shorter periods, although this varies somewhat from site to site. It should be noted that the bathymetry of the Trough and the present study are quite different. The bathymetry of the Japan Trench is extreme, but has a fairly simple geometry. Whereas the Trough bathymetry is less severe, but somewhat complicated due to the broad and heavily faulted continental borderland.

5. Impedance polarization diagrams and phase tensor ellipses

Fig. 4 shows the impedance polarization diagrams (e.g., Berdichevsky and Dmitriev, 2008) and phase tensor ellipses (Caldwell et al., 2004) for all seafloor stations. The impedance polarization is a metric for evaluating the dimensionality of the conductivity structure and the geologic strike. The polarizations are largely direction independent for sites s05–s09 at periods less than about 100 s, indicating a predominantly 1D shallow conductivity, whereas the deeper sites (s01–s04) exhibit a roughly north–south polarization at these same periods, indicating a 2D strike that is parallel to the local trend of the Japan trench. At longer periods all sites show a rotation of strike to the northwest-southeast direction. The diagonal impedance component Z_{xx} also increases in size at long periods as the impedances become more polarized. Although not shown, the impedance tensors for the seafloor stations exhibit skews (Swift, 1986) of less than 0.2, thus implying that the data are devoid of large 3D inductive effects. There are a few exceptions to this with skews as large as 0.45 for data at 1000–5000 s period at sites s01 and s04. Overall, the impedance tensor polarizations suggest the short period data are compatible with a 2D strike that is roughly aligned with the local north–south trend of the Japan trench, associated seafloor topography and the nearby coastline, whereas the increase in polarization and the rotation for the longer period data (>100 s) indicate a change in geologic strike. Given that seafloor MT data are sensitive to conductivity variations both beneath the measurement site as well horizontally distant, the long period rotation in strike is likely due to the strong 3D conductivity contrast associated with the bend in the trench strike only 100 km to the north of our array, as it transitions from the roughly north–south strike of the Japan trench to the southwest-northeast strike of the Kuril trench.

MT phase tensors are a recent innovation that are immune to the galvanic distortions such as static shifts that can strongly affect land MT measurements (Caldwell et al., 2004). While regional and coastal seafloor topography is known to cause galvanic shift of TM mode measurements (e.g., Heinson and Constable, 1992; White et al., 1997; Constable et al., 2009), there have been been no defini-

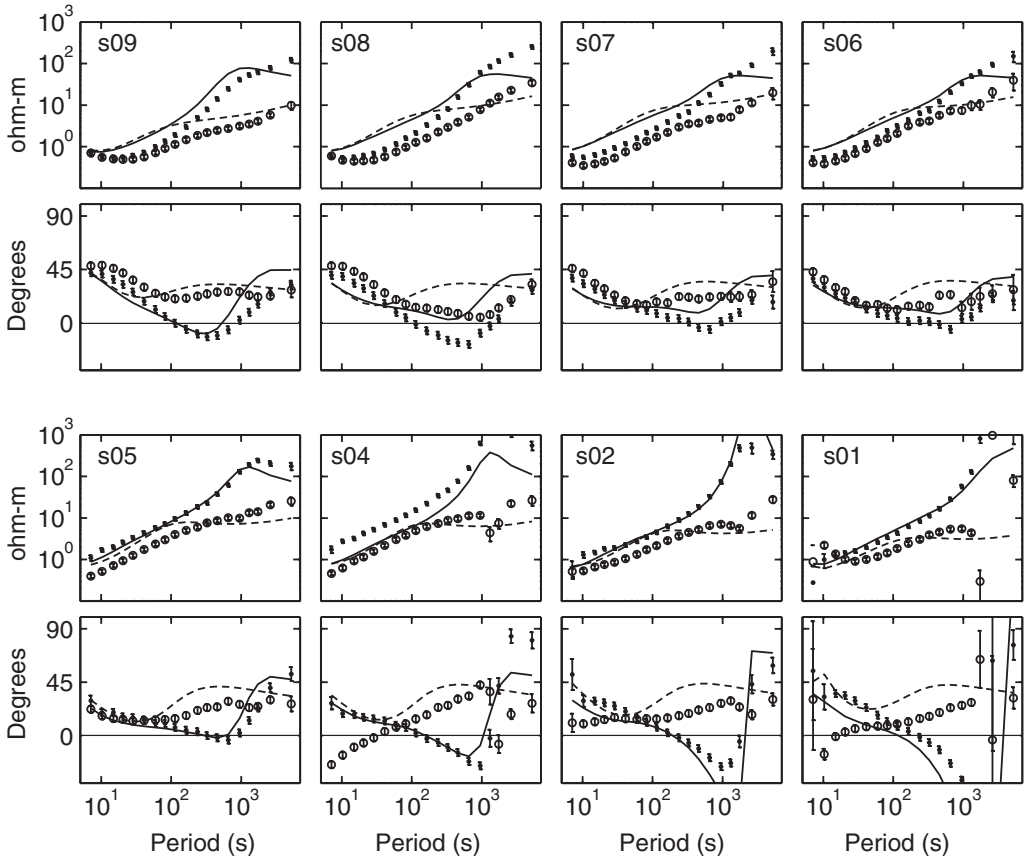

Fig. 3. Apparent resistivity and phase responses for the eight seafloor MT stations. The Z_{xy} (dots) and Z_{yx} (circles) data are shown along with corresponding TE and TM mode forward responses (lines) for the 2D model shown in Fig. 6, illustrating that much of the observed difference between the responses, including negative TE phases, cusps in the long period TE apparent resistivity, and depressed TM mode apparent resistivity can be simply explained as topographic distortion of the MT responses.

tive studies documenting static shifts in marine MT data, at least in the conventional land MT sense that static shifts are caused by small scale near-surface conductivity variations. One explanation for the absence of static shifts is the ubiquity of nearly uniform conductivity surrounding seafloor MT sensors, both in the form of the conductive seawater and the porous conductive sediments on the seafloor. Regardless, phase tensors are still worthwhile to consider for marine MT since they represent an independent metric of data variations across the array and may be helpful in cases where seafloor data have strong galvanic distortion from TM mode coast effects. In Fig. 4, sites s05–s09 exhibit nearly circular phase tensor ellipses at short periods, in agreement with the impedance tensors indicating a shallow 1D conductivity. However, the phase tensors become highly polarized at long periods due to the large split between the Z_{xy} and Z_{yx} phases. These strongly polarized phase ellipses are correlated with the band of large negative phases at periods of 114 s and longer. Additionally, there is a strong ellipse rotation at longer periods, again suggesting a rotation in geologic strike or the presence 3D distortions. Fig. 4 shows that the phase tensor strike angles (Caldwell et al., 2004) also suggest a predominantly north-south strike for the short period data and a strike rotated to the northwest-southeast for the long period data.

Given the results of the impedance polarization and phase tensor analyses, we determined that the best 2D strike direction is the north-south direction, in agreement with the large first order conductivity contrast between the seafloor and ocean locally around the receiver array. However, care will need to be taken for 2D examination of the longer period data since there is a rotation in strike by about 30° to the northwest.

6. Inter-station magnetic and electric transfer functions

Fig. 5 shows the magnetic transfer functions **M** and electric transfer functions **T**. Since the observed tensors are diagonally dominant with off-diagonal terms at least 10 times smaller, only the diagonal terms are shown. These responses are dominated by the large attenuation of the short period data due to the conductive overlying seawater, with the deepest sites experiencing the largest attenuation, in good agreement with 1D theoretical predictions (e.g., Chave et al., 1991). The magnetic transfer tensor component M_{yy}, corresponding to the east–west magnetic field, exhibits a striking local minimum in amplitude and a rapid phase shift of over 100° at periods around 1600 s for the three deepest sites. Conversely, the electric transfer tensor component T_{xx} does not display such extreme behavior, although there is a weak local minimum in amplitude at similar periods. We can now explain the cusps in the Z_{xy} apparent resistivity and corresponding negative phases as arising from the variation of H_y. Since for a 2D geometry $Z_{xy} = E_x/H_y$, when H_y reaches a minimum at around 1600 s the corresponding Z_{xy} apparent resistivity will contain a positive cusp. Conversely, the M_{xx} and T_{yy} transfer functions are well-behaved and do not display these features, in agreement with the stable behavior of the corresponding Z_{yx} responses.

7. Numerical modeling of 2D coast effect distortions

In order to elucidate the nature of the severe distortion of the MT responses, we carried out numerical forward modeling experiments on 2D models of the coastline and seafloor along the survey profile. A 1000 km long transect of topography was discretized into

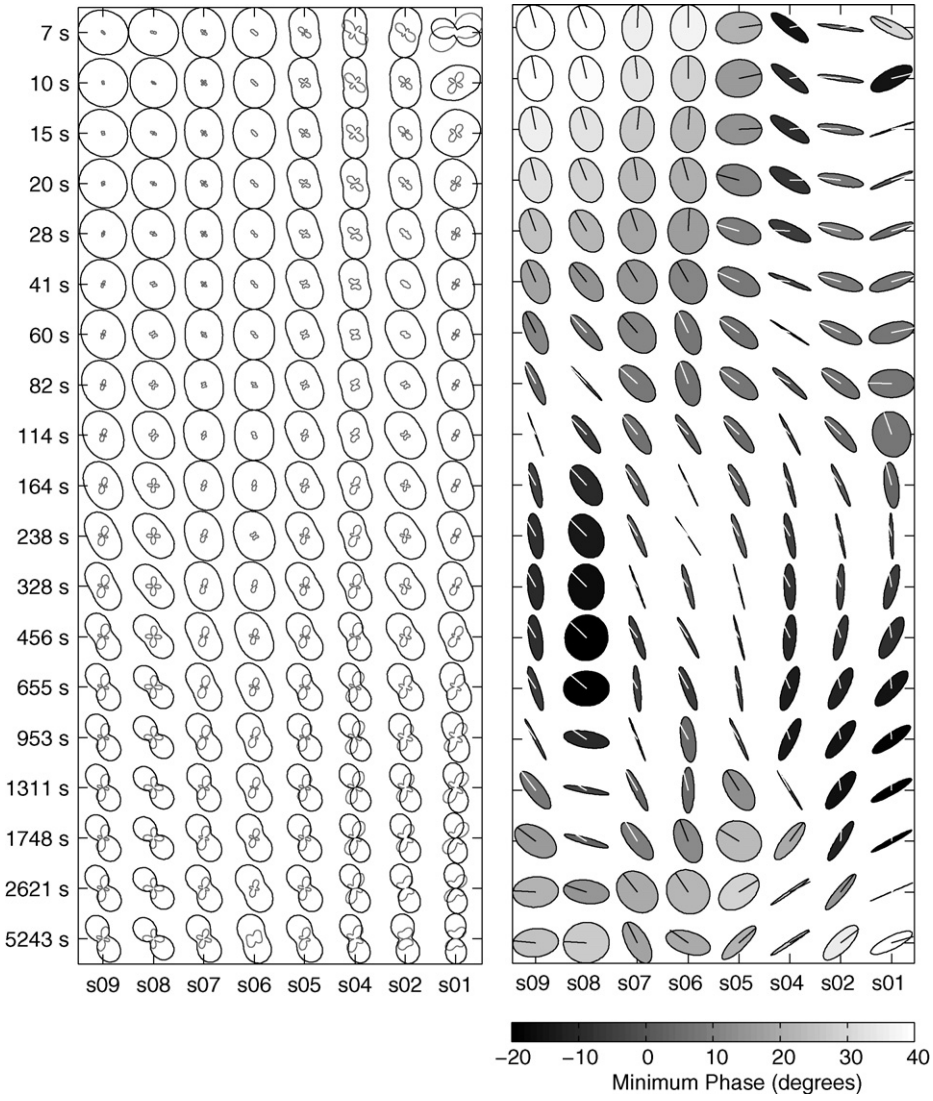

Fig. 4. Impedance polar diagrams (left) and phase tensor ellipses (right) for all stations as a function of period. The polar diagrams show the relative magnitude of Z_{xx} (gray) and Z_{xy} (black) as a function of geographic orientation (north = up). The phase tensor ellipses are shaded according to the minimum phase angle and clearly show the prominent zone of negative phases for data at periods of about 100–1000 s. Lines on the phase tensors indicate the regional phase strike angle (Caldwell et al., 2004). Each plot has been normalized to unit magnitude along the maximum polarization.

points spaced every 5 km and used to create an unstructured triangular finite element mesh of the 2D topography of the Japan island, trench and deep-ocean abyssal plain. The entire model mesh was made more than 5000 km wide to ensure distortions from the coastline topography in the central portion did not corrupt the 1D boundary conditions applied along the sides of the model. The model was divided up into four regions: air, ocean, seafloor sediments and a uniform underlying half-space, as shown in Fig. 6. The sediment thickness is based on seismic reflection and refraction surveys that found a ~1 km thin veneer of Neogene-Quaternary sediments overlies an Oligocene unconformity (Tsuru et al., 2000; Hayakawa et al., 2002; Ito et al., 2004). A sediment resistivity of 1 ohm-m was assigned based on the high porosities predicted by the low seismic compressional velocities of 2–3 km/s. MT responses were computed using a parallel goal-oriented adaptive finite element method (Key and Ovall, in revisions). After some trial-and-error, we found that a background resistivity of 200 ohm-m produces forward responses that match the main trends of the observed responses, as shown in Fig. 3. The model responses show the negative TE mode phases, the cusp in TE resistivity observed for the deepest sites and the rapid increase in TE phase angle at long periods. The model responses also reproduce some of the TM mode depression observed in the data. Fig. 5 shows the inter-station transfer functions for the 2D model are in good agreement with the main trends of the observed data, reproducing the minimum in the M_{yy} amplitude and the corresponding large phase shift at around 1600 s period.

The electric field transfer functions for the 2D model illustrate behaviors related to the inductive and galvanic distortions from the coastline. At long periods, the TM mode T_{yy} responses show a large galvanic distortion, consisting of a frequency independent shift between the amplitude responses for each station, with the absence of a corresponding phase shift. Conversely, the the TE mode T_{xx} model responses vary both in amplitude and phase at long periods, indicating inductive distortion. Comparison with the observed data shows that the T_{yy} data have a distortion that appears largely galvanic, as expected for the local topography and coastline. Somewhat unexpectedly the T_{xx} data appear to have a galvanic distortion that is larger than the T_{yy} data, with significant shifts between the amplitude responses for each site and a lack of corresponding phase distortion. This can be explained as galvanic distortion from the large bend in the regional topography where the Japan trench

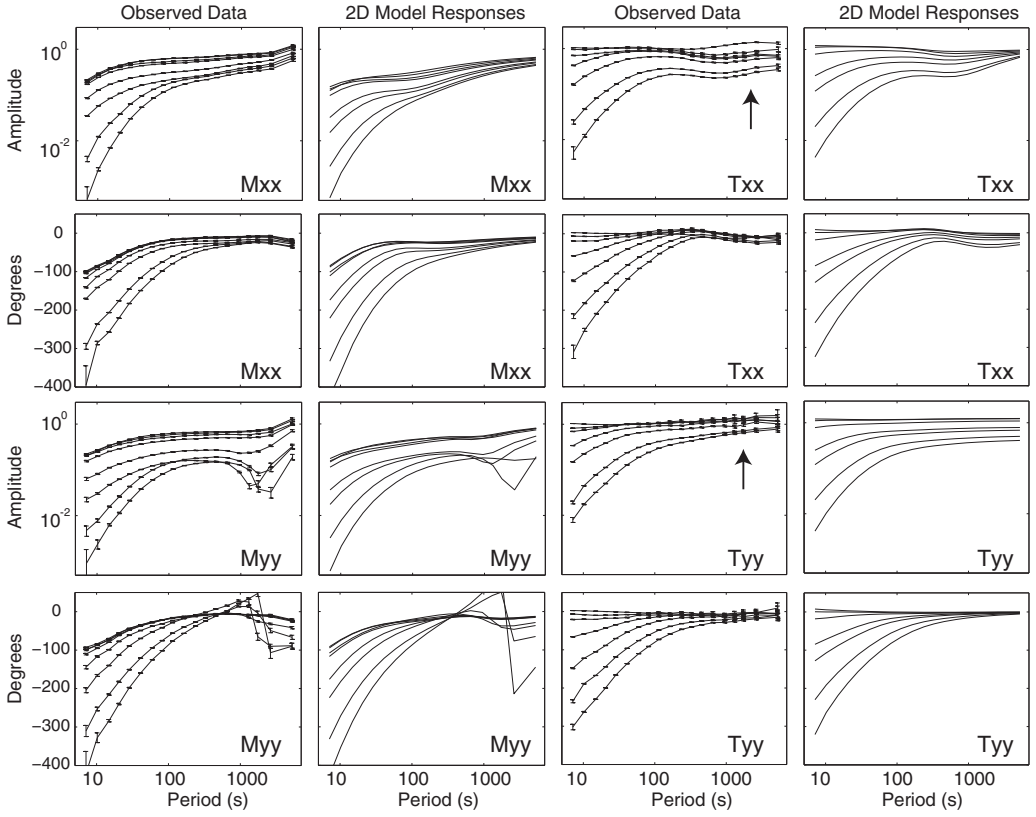

Fig. 5. Observed and modeled inter-station transfer functions. Magnetic transfer functions **M** were computed between the seafloor sites and the land remote site, while the electric field transfer functions **T** used s09 as the reference. The ordering of the curves corresponds to the depth of each site, with the transfer functions for s01 showing the largest attenuation at short periods. The 2D model responses are from the simple model shown in Fig. 6. Since the observed tensors are predominantly diagonal with off-diagonal terms at least 10 times smaller, only the diagonal *xx* and *yy* terms are shown. Black arrows indicate the electric field transfer function amplitudes exhibiting a frequency independent galvanic shift at long periods.

joins the Kuril trench and islands, which are nearly perpendicular to the T_{xx} component and hence allow for TM mode-like galvanic distortions. This is further evidence (in addition to the impedance polarizations and phase tensors) to support the idea that the long period data are sensing 3D effects due to a rotation in strike, with the implication that the interpretation of the long period data will require the ability to simulate the 3D topography on a regional scale around the survey area.

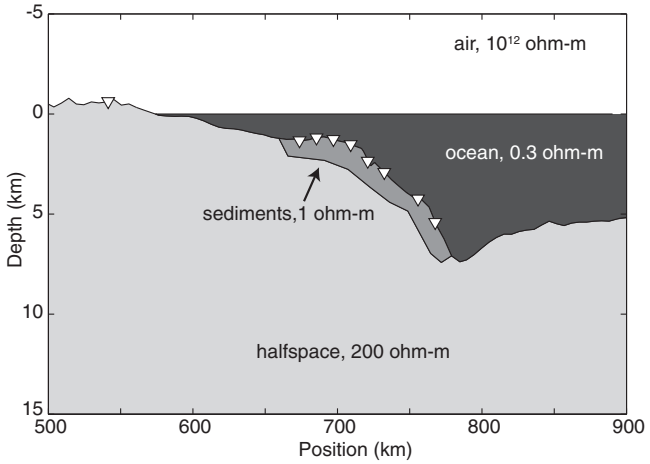

Fig. 6. A simple two-dimensional model consisting of the island and seafloor topography along the MT profile, extending through the trench and onto the abyssal plain. The MT responses of this model are shown in Fig. 3 and the inter-station transfer functions are shown in Fig. 5. Only the central region of the model is shown here. White triangles are the locations of the seafloor MT stations.

The fact that such a simple 2D model is able to reproduce the many data distortion features serves to illustrate the severity of the coast effect, with strong implications for the interpretation of marine MT data affected by such distortions. The sensitivity to the seafloor half-space resistivity is demonstrated in Fig. 7, which shows the TE mode response and the M_{yy} transfer function at site s01 as a function of the underlying half-space resistivity. When the seafloor is 1 ohm-m, nearly as conductive as the seawater, there is no distortion of the MT response nor the magnetic transfer function. However, as the seafloor resistivity increases the response becomes increasingly distorted, as indicated by large negative phases and even phase wrapping through 360° of variation. The degree of the TE mode distortion as a function of resistivity is similar to results from an earlier model study presented in Constable et al. (2009). The M_{yy} transfer function distortion shown here illustrates how this unusual TE mode response behavior is largely due to a TE magnetic field distortion that consists of an amplitude minimum and rapid phase change at a characteristic frequency. A corresponding study of the TM mode coastline distortion shows that it is predominantly manifest as a downward galvanic shift in the apparent resistivity (Constable et al., 2009).

7.1. Insights from the electric field and Poynting vectors within the earth

While the above examples document that the TE mode distortion arises as a magnetic field phenomenon, they do not provide

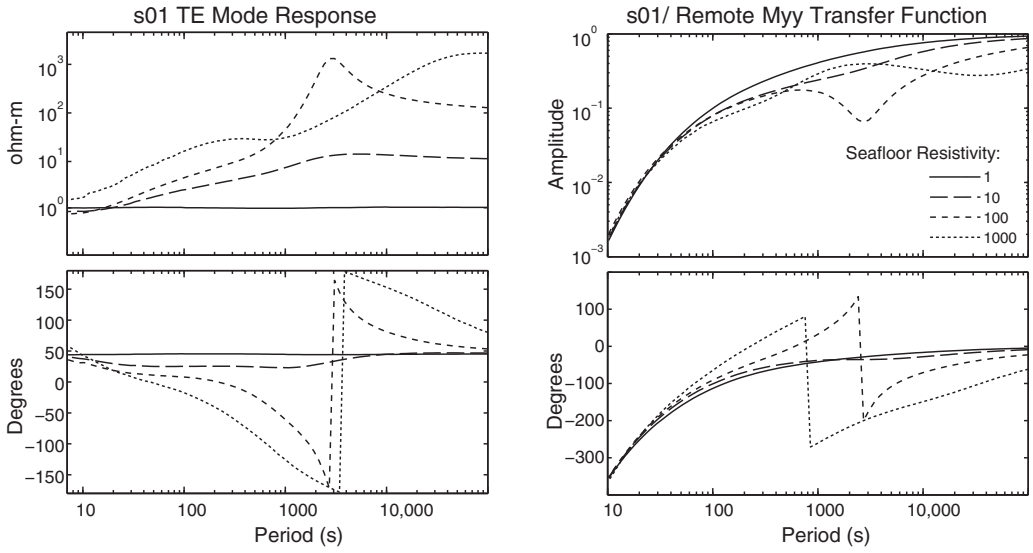

Fig. 7. The TE mode MT response and M_{yy} transfer function at site s01 as a function of the underlying seafloor half-space resistivity.

much insight on its physical cause. Some clarity can be gained by examining how the TE mode fields vary within a cross section of the 2D model. Fig. 8 shows the TE mode electric field amplitude throughout the central region of the model domain for periods of 100, 1000 and 10,000 s. As expected, the TE electric field diffuses through the resistive Japan island with little attenuation, whereas the conductive seawater produces a strong attenuation of the field diffusing through the ocean, which is particularly evident in the 100 s section. Because of the continuity condition, the strike aligned electric field diffusing through the island must decay laterally to the attenuated levels on the deep ocean seafloor, thus leading to a strong lateral gradient in the electric field. In some cases, the electric field contours steepen past vertical, for example at the base of the trench for the 100 and 1000 s sections. The extreme lateral gradient of the TE electric field from land to the deeper regions of the seafloor was pointed out in our earlier study as a contributing factor for the TE coast effect distortion (Constable et al., 2009).

Even greater insight is gained by visualizing the diffusion path of the downward propagating TE magnetotelluric field using the time-average of the complex Poynting vector (e.g., Stratton, 1941):

$$\bar{\mathbf{S}} = \frac{1}{2} Re(\mathbf{E} \times \mathbf{H}^*), \tag{9}$$

where $\mathbf{H}^*$ is the complex conjugate of the magnetic field. For the 2D TE mode, this expands into

$$\bar{\mathbf{S}} = \frac{1}{2\mu\omega} Re\left(iE_x \left(\frac{\partial E_x^*}{\partial y}\hat{y} + \frac{\partial E_x^*}{\partial z}\hat{z} \right) \right), \tag{10}$$

where μ is the magnetic permeability, ω is the angular frequency, $i = \sqrt{-1}$ and $\hat{y}$ and $\hat{z}$ are unit vectors in the y and z directions. This states that the direction of energy flow depends on the product between the TE electric field and its spatial gradients in the y–z plane, rather than just its gradient as might be incorrectly inferred from the bending of the TE electric field contours shown in Fig. 8. The right column of Fig. 8 shows streamlines computed from $\bar{\mathbf{S}}$. The streamlines clearly show how the bathymetry and coastline act to distort the incident magnetotelluric field. At 100 s period, the regions far from the coastline and seafloor topography have streamlines showing the energy is diffusing vertically into the ground (as is expected for typical MT induction), whereas around the coastline and at the base of the deep trench, the energy appears to curve through the ground and diffuse back up to the seafloor. This effect becomes more pronounced at 1000 and 10,000 s period. While this appears similar to refraction phenomenon where a ray path bends as it traverses media of different physical properties, we note that the seafloor in our model study has a uniform conductivity in this region so that refraction is not occurring. Instead, the curvature of the diffusing electromagnetic field can be interpreted as the result of strong inductive coupling between the conductive ocean and the resistive seafloor topography.

For comparison, the TE mode phases are also shown in each section. These show that the phases reach extreme values only in the regions where the TE energy is diffusing back up to the seabed instead of the typical downward trajectory. At 100 s period, most of the anomalous TE phases are negative, whereas at 10,000 s the TE phases reach up to 180°, both in agreement with our observed data. Evidently, the extreme phase values observed in our data result from interference between the TE electromagnetic field that diffuses down through the conductive ocean and the less attenuated field that diffuses laterally and upward through the resistive seafloor.

While the streamlines at 1000 and 10,000 s appear to be regionally distorted over the entire forearc slope, the distortion at 100 s period appears to be localized around two specific regions: the vicinity of the coastline and a second region where the bathymetry is very steep near the bottom of the trench. This suggests that at short periods the coast-effect and topographic distortion is due to local conductivity gradients, whereas at longer periods where the skin-length is much larger the distortion arises from regional coastlines and the overall integrated seafloor topography. This supports our explanation for the rotation in strike seen in the impedance polarizations and phase tensor ellipses shown in Fig. 4. Given the strong bend in the trench axis only 100 km to the north of the survey line, it is likely that the impedance strike rotation is arising from topographic distortion from the 3D shape of entire trench margin. There may also be additional distortion from 3D subsurface conductivity associated with the subducting slab and volcanic systems observed onshore. However, the first order conductivity contrast between the seawater and seafloor suggests that topographic effects are probably the primary cause of the strike rotation.

Another aspect of the lateral and upward flow of energy shown in Fig. 8 is that the TE coast effect distorted MT fields measured on the seafloor can be sensitive to the seafloor conductivity along a wide swath of the continental margin. For example, at 1000 s period an MT sensor located over the middle of the continental slope can

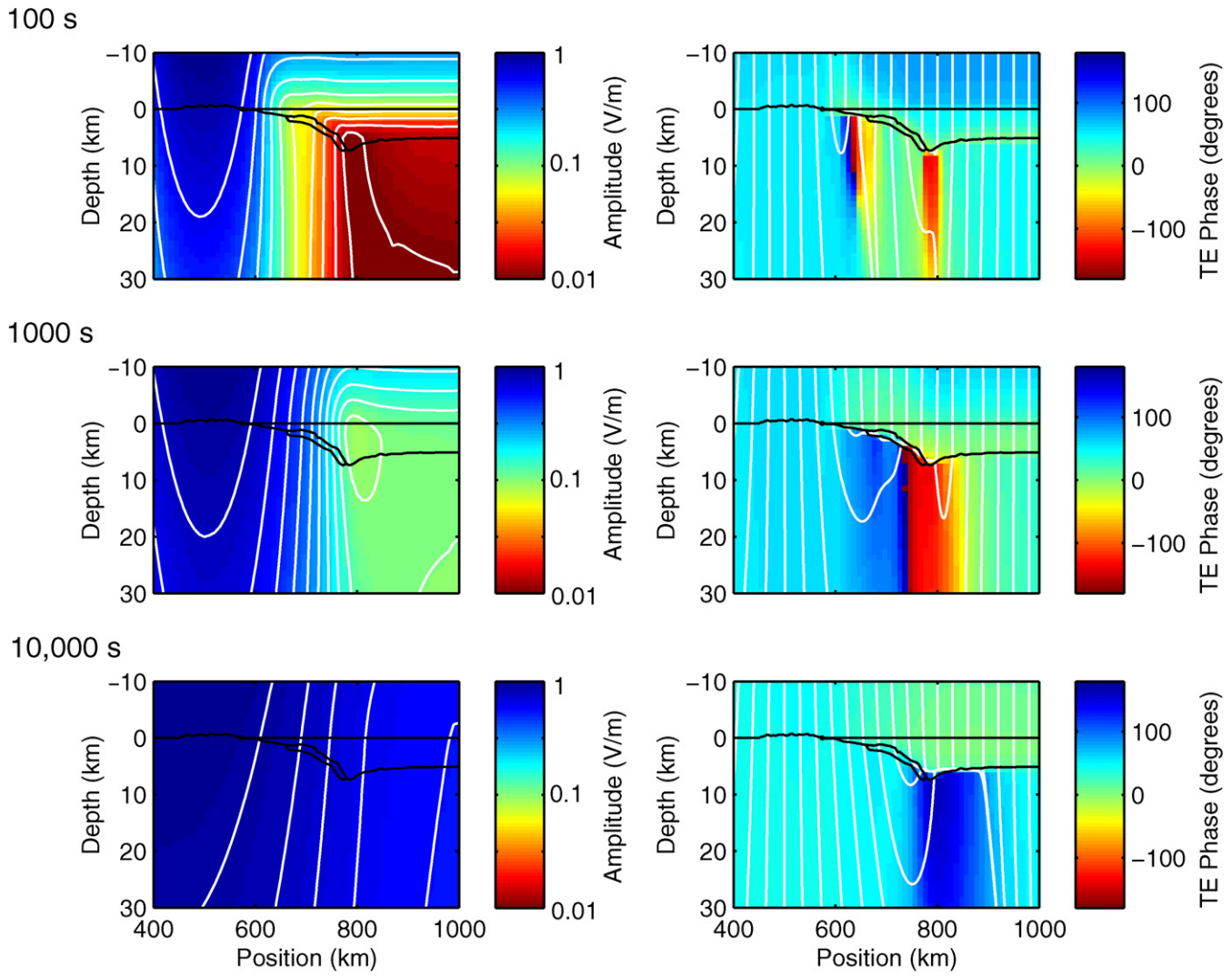

Fig. 8. The TE mode coast effect as elucidated by the strike parallel electric field amplitude (left column) and the TE response phase (right column), shown for periods of 100, 1000 and 10,000 s. White lines show electric field amplitude contours (left column) and streamlines of the time-averaged complex Poynting vector (right column).

be sensitive to the integrated seafloor conductivity all the way to the coastline, as shown by the streamlines in Fig. 8.

8. Interpretation of coast-effect distorted data

When topographic distortions are present in seafloor magnetotelluric data, there are two methods commonly used for interpretation. The first method involves directly including the topography in the numerical grid used for forward and inverse modeling, typically implemented with either finite difference or finite element methods (e.g., Key and Constable, 2002; Li et al., 2008; Constable et al., 2009). However, accurately meshing complicated bathymetry can present a challenging grid design problem that often leads to very large discretizations when using structured rectangular modeling grids, particularly for accurate computations at the short periods measured by broadband instrumentation. This has spurred the development of modeling techniques that can accommodate seafloor and coastline topography with much sparser numerical grids. Baba and Seama (2002) implemented a conductivity averaging approach to allow for a uniformly spaced rectangular finite-difference modeling grid, while Key and Weiss (2006) developed an adaptive finite element method that uses unstructured triangular elements that readily conform to complex topography. Additional finite element methods utilizing unstructured grids are presented in Franke et al. (2007), Li and Key (2007), Li and Pek (2008) and Key and Ovall (in revisions).

An alternative approach treats the topographic effects as removable distortions (e.g., Heinson and Lilley, 1993; Nolasco et al., 1998; Baba and Chave, 2005; Matsuno et al., 2007). In this case, the forward response of the topography is similarly computed with finite difference or finite element methods, or for very long periods using thin-sheet methods, but it is then combined with the response of a flat seafloor model in order to estimate electric and magnetic topographic distortion tensors for each seafloor station. With knowledge of the distortion tensors, topographic effects are removed from the observed MT responses, which can then be modeled using a numerically simpler modeling grid with a flat seafloor. See Matsuno et al. (2007) for a recent discussion on the various distortion tensor formulations that have been proposed.

While the distortion removal approach has proven effective for long period MT data collected in the deep ocean abyssal plain where topographic distortions can be effectively decoupled from the deeper mantle resistivity under investigation (e.g., Matsuno et al., 2007), the large lateral field gradients experienced close to the continental margin makes their use problematic for our survey data, particularly since the coast effect distortions are strongly coupled to the unknown continental margin seafloor resistivity. Another obvious difficulty is the choice of the flat seafloor depth

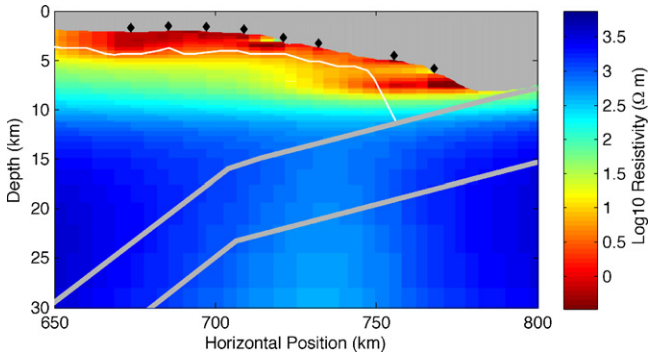

Fig. 9. Occam2DMT inversion model fitting the data to RMS 1.0. Seafloor MT stations are shown as black diamonds. White lines show the base of low velocity sediments imaged in a seismic survey (Ito et al., 2004). Thick gray lines show the oceanic crust being subducted beneath the forearc (Fujie et al., 2006). To minimize potential corruption from long period 3D effects, only data at periods less than 500 s were inverted.

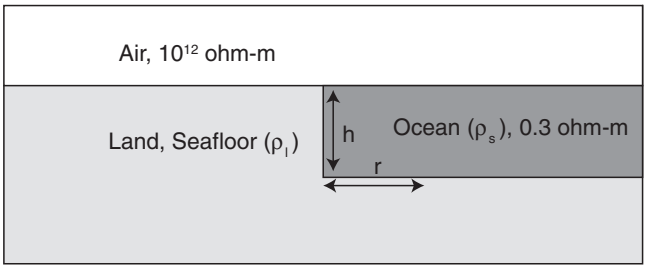

Fig. 10. Model parameterization for studying the coast effect as a function of seafloor resistivity ρ_l, ocean thickness h and distance r from the coast.

required for estimating the topographic distortion tensors. For surveys in the deep ocean abyssal plain, the average sea depth is effective, but for surveys across the continental slope there is no obvious choice for the corrected seafloor depth, particularly when receivers are positioned across a wide range of depths, for example from the shoreline to the deep ocean seafloor.

For the survey data considered here, the target objective is to image the conductivity from the seafloor down to the subducting plate boundary at depths of 10–30 km. Because the coast effect is strongly coupled to this relatively shallow region, a reliable interpretation can probably be achieved only through direct topographic modeling approaches, rather than currently available methods for distortion removal. While a thorough analysis of the entire data set requires 3D modeling of the Japan and Kuril trench topography, the dimensional analysis presented earlier indicates that the data at shorter periods are compatible with 2D structure aligned perpendicular to the survey profile. Therefore, we perform 2D interpretation on a reduced data set consisting of the TE and TM mode responses at periods less than 500 s.

We used the standard Occam2DMT inversion algorithm (deGroot Hedlin and Constable, 1990). Occam2DMT is built around a finite element forward modeling code capable of handling seafloor topography using structured triangular elements (Wannamaker et al., 1987) and that utilizes a reciprocity method for rapid computation of the Jacobian (de Lugao and Wannamaker, 1996). The model was parameterized into 3592 free parameters and a total of 416 apparent resistivity and phase data were inverted after applying a 20% error floor. We note that this subjective error floor is significantly larger than many of the statistical variances of the computed MT responses, yet it serves to pad the 2D inversion from over-fitting 3D distortions in the data. The inversion started from a 10 ohm-m halfspace resistivity and after 10 iterations converged to an RMS misfit of 1.0. The resulting conductivity model is shown in Fig. 9.

The inversion model contains a layer of conductive sediments over a resistive forearc mantle wedge and subducted seafloor. Comparison with the basal depth of the sediments as mapped with seismic data shows that even a few sites of MT data do a reasonably good job at mapping the sediment thickness. Although we have truncated the data to periods less than 500 s, simple skin-length arguments suggest that the data are still sensitive to structure at the depth of the plate boundary. The lack of any conductivity anomalies in this region implies a low bulk porosity and fluid content for the subducting ocean crust in this region. Seismic velocities immediately beneath the subducted plate boundary are consistent with those of normal layer 2 oceanic crust, although at these depths they are poorly resolved (Ito et al., 2004). We have certainly taken a conservative approach to inversion of this data set given the known rotation in strike at longer periods. It is worth pointing out that conductivity variations along the subducted plate boundary, if present, may be below the conservative 20% error floor imposed on the data. Future analysis of this data set that incorporates 3D topographic modeling is required to make a more conclusive assessment of the deeper plate boundary structure. However, our simple 2D topography inversion approach demonstrates a methodology for effective imaging of crustal conductivity variations on the continental margin. Finally, there may be cases where highly 3D bathymetric variations distort seafloor MT data such that 2D interpretation is not valid and full 3D modeling is required, even for imaging shallow crustal structure.

9. Distortion with distance from the coast

The previous sections have characterized the TE mode distortion on the continental margin specifically in our survey area. It is now worthwhile to consider how this distortion manifests in the broader context of seafloor MT soundings at a variety of ocean depths, distances from coastlines and for variable seafloor resistivity. Fig. 10 shows a simple 2D model consisting of a coastline of height h, a uniform land and seafloor resistivity ρ_l, and seafloor MT stations at a distance r from the coastline. We computed MT responses for this model using a parallel adaptive finite element method (Key and Ovall, in revisions) at periods of 1–100,000 s, corresponding to the combined period range of typical broadband and long period instrumentation. Seafloor MT stations were spaced logarithmically at distances r of 100–1,000,000 m from the coastline. Responses were computed for ocean depths h of 100, 1000 and 4000 m and seafloor resistivity ρ_l set to 10, 100 and 1000 ohm-m, thereby covering the range of ocean depths and seafloor resistivities typically encountered in continental shelf and deep ocean MT surveys. The resulting TE and TM mode responses are shown in Fig. 11.

There are distinct similarities and differences between the TE and TM mode responses. The responses are similar in that the largest distortions occur for the 4000 m ocean with a 1000 ohm-m seafloor, and that most of the distorted response is present at offshore distances that are less than a skin-length in the seafloor, although at the shortest periods the distortions are present to greater distances. Conversely, the 1 ohm-m seafloor results in almost no distortion for any of the ocean depths since the seafloor conductivity is close to seawater, representing only a subtle 2D contrast. The large distortions are expected for the more resistive seafloor models since they represents significant 2D contrasts. The size of the distortion and its bandwidth increase with the ocean depth for both TE and TM modes and both modes contain depressed apparent resistivities, but the TE mode has a narrow positive peak in apparent resistivity at some distance, after which the distortion subsides at greater distances. Conversely, the TM mode does not

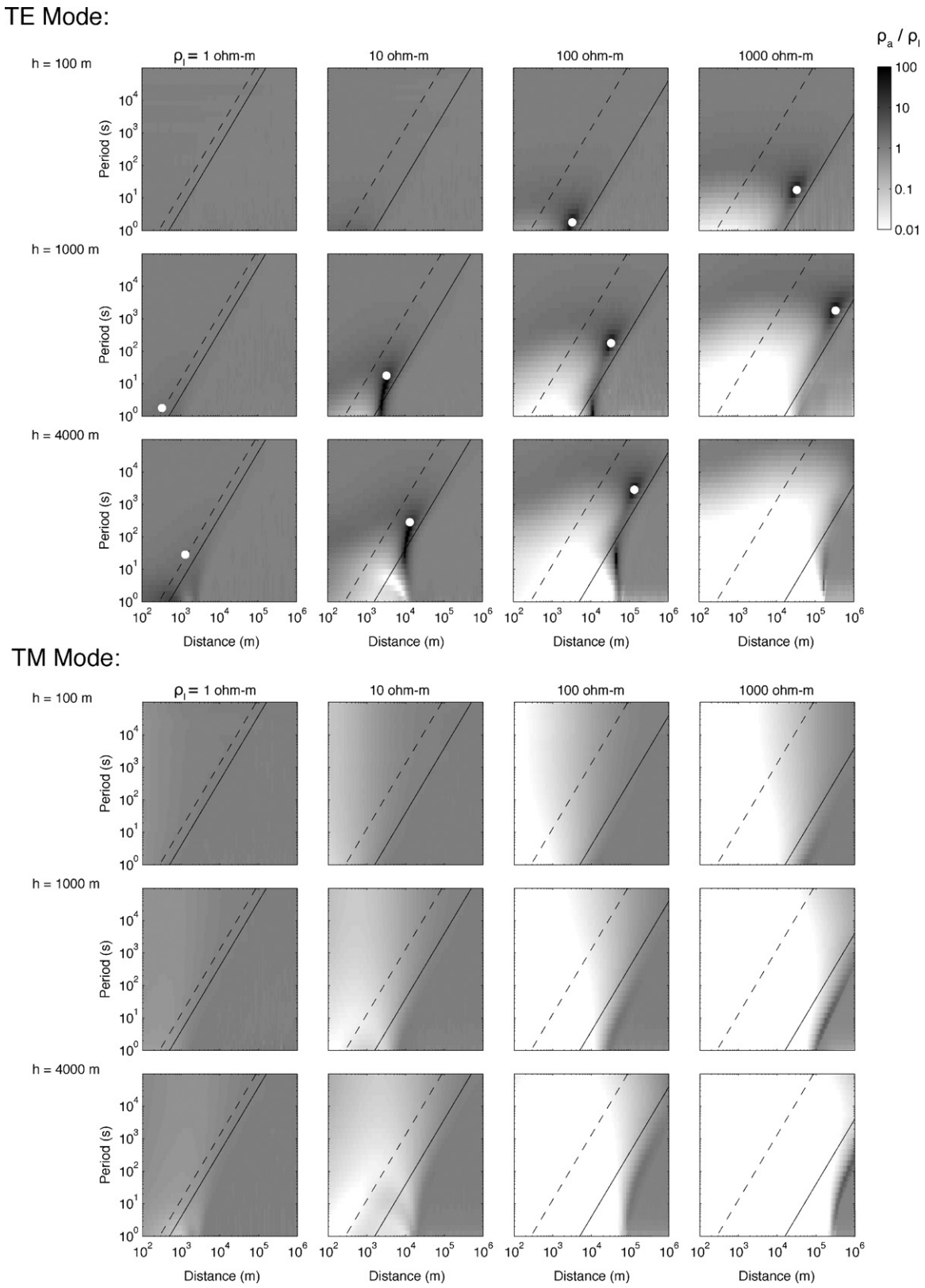

Fig. 11. The distortion of seafloor apparent resistivity responses as a function of ocean height, seafloor resistivity and coastline distance. The model parameters are shown in Fig. 10. The responses have been normalized by the seafloor resistivity so that black and white colors correspond to large distortions while gray colors indicate little or no distortion. The dashed and solid lines show the skin-length for the 0.3 ohm-m ocean and the variable seafloor resistivity, respectively. The white dots show the predicted location of the TE mode resistivity peak based on the empirically derived scaling model given in the text.

contain a peak in resistivity, although the 1000 ohm-m seafloor responses exhibit a small increase in resistivity along a narrow ridge at long ranges. The depressed TE and TM mode resistivities can be in excess of 100 times smaller than the halfspace value, while for a given model the TM mode has a significantly more depressed response than the TE mode. The TM distortion only varies weakly with period and extends across the entire period bandwidth of the computations, indicating it is predominantly a galvanic distortion. Conversely, the TE distortion varies strongly with frequency, with the distortion largely absent at the longest periods. The transition between distorted and undistorted TE responses varies systematically with ocean depth and seafloor resistivity. This period dependence is consistent with the TE distortion being an inductive effect as required by the TE mode physics. Another difference between the modes is that the TM distortions vary slowly with distance from the coast, whereas the TE distortions can vary substantially, with the largest TE distortions found at some distance far offshore.

The peak in TE apparent resistivity remains above the halfspace values over a fairly narrow range of distances from the coastline. For example, the 1000 m ocean model with a 100 ohm-m seafloor has a peak at distances of 5–20 km offshore, with a center at about 10 km offshore. The peak extends over a much wider range of periods, but this is somewhat complicated by a crescent shape to the peak for the deep ocean models with more resistive 100 and 1000 ohm-m seafloors. In all cases where a peak is present, it is above the halfspace values for at least a decade of periods.

Interestingly, the strong peak in the distorted TE apparent resistivity occurs systematically at a distance of just under half a skin-length in the seafloor. The peak moves to farther ranges and longer periods as the ocean depth and seafloor resistivity increase. From the range of parameters shown in Fig. 11, the peak location in the range and period space appears to depend linearly with seafloor resistivity, while its period depends on the square of the ocean depth and its range depends linearly on ocean depth. Empirically, the following equations have been found to accurately predict the period and range of the TE response peak:

$$T = a\frac{\rho_l h^2}{\rho_s^2}, \tag{11}$$

$$r = b\frac{\rho_l h}{\rho_s}, \tag{12}$$

where $a = 1.88 \times 10^{-7}$ and has the same units as magnetic permeability and the dimensionless quantity $b = 0.091$. Although not shown here, these equations were tested on two other models with artificial ocean resistivities ρ_s set 10 times larger and smaller than the realistic 0.3 ohm-m value used in here. In both cases, the above equations accurately predict the location of the TE response peak, which is located in a new location in range-period space according to the dependence on ρ_s given in the equations above. The simple form of these equations and their reliability for predicting the TE resistivity peak over the large range of model parameters given here suggests that there may be a simple underlying theoretical formulation for this aspect of the TE mode distortion that is awaiting future discovery.

While this 2D model study is undoubtedly oversimplified in comparison to the complex topography and seafloor of real continental margins, we note that its prediction for the TE mode peak agrees strikingly well with real data we have collected. For example, the San Diego Trough has a 1000 m ocean depth, with 2D inversion recovering an average seafloor resistivity of 100 ohm-m. Eq. (11) predicts a TE response peak of 200 s, in excellent agreement with the observed peak at the same period. Similarly, Eq. (12) predicts the peak occurs around a range of 30 km offshore, in agreement with the distance of the Trough from the San Diego coast. Application to the data considered here predicts a TE mode peak centered around 180 km offshore, in agreement with the TE peak observed at 150–200 km distance offshore at sites s01, s02, s04 and s05. Data collected at the mid-ocean ridge along the northern East Pacific Rise do not contain any peaks in apparent resistivity, despite seafloor resistivities in excess of 500 ohm-m and ocean depths of 2500 m (Key and Constable, 2002). This is simply due to the nearest coastline being over 1000 km distant. Likewise, broadband data collected at Gemini Prospect in the Gulf of Mexico in 1 km ocean depths about 100 km offshore contains no evidence of coast effect distortion since the 7 km thick continental shelf sediments are almost uniformly 1 ohm-m (Key et al., 2006). The reliability of these equations suggests that the range and period location of the TE response peak could be well predicted before a survey if the seafloor resistivity is known a priori. Conversely, if one observes a peak in the TE resistivity, since the distance offshore, the ocean depth and seawater resistivity are well known quantities, equation 11 or 12 could be used to estimate the bulk seafloor resistivity. However, there will certainly be more complicated situations where these equations may not be valid, such as where coastlines are 3D or in regions with significant 2D and 3D subsurface conductivity variations.

The high level of distortions produced by such a simple model geometry demonstrates that the coast effect observed in both the San Diego Trough and the data considered here are probably ubiquitous features of seafloor MT soundings near thinly sedimented continental margins, rather than spurious features present only for the particular coastline and seafloor topography of these survey regions. Another implication is that the depressed apparent resistivities may extend to several hundred or even thousands of kilometers offshore for a very resistive seafloor, even at relatively short periods. If care is not taken to properly include the coast effect depression in numerical modeling efforts, the resulting interpretation of such distorted data would result in a gross underestimation of the mantle resistivity. Heinson and Constable (1992) came to a similar conclusion with thin-sheet modeling of the coast effect for long period marine MT data (>1000 s). A final cautionary warning regards the interpretation of the TE apparent resistivity cusp, which if not recognized and properly accounted for with 2D or 3D numerical methods could result in a large overestimation of seafloor resistivity.

Certainly there may be cases where the offshore topography is highly 3D, or where substantial leakage paths may alter the magnitude of the coastline distortion. However, we are not aware of any MT studies documenting the presence of such leakage paths, although this may be due to the relative sparsity of marine MT observations in the ocean basins worldwide. There may also be coast-effect like distortions produced by other large-scale seafloor topographic features such as transform offsets, fracture zones, small islands and seamounts.

10. Conclusions

The strong galvanic and inductive distortions of our broadband marine MT data collected on the forearc of the Japan trench demonstrate the severity of the coast effect along resistive continental margins. While it has been known for some time that the TE mode coast effect is largely due to a magnetic field distortion (Ferguson, 1988), our Poynting vector analysis provides new insights on this phenomenon. The Poynting vectors show how the normal downward diffusion path of the MT plane-wave is inductively distorted by the resistive seafloor topography, so that energy diffusing down through the onshore section bends laterally and then back upwards beneath the continental margin. This results in a zone of interference along the seafloor where energy diffusing down through the ocean collides with energy propagating upwards from beneath

the seafloor, producing anomalous TE mode responses containing cusps in apparent resistivity and phases that wrap out of quadrant. The characteristic frequency and position of the TE mode apparent resistivity cusps are determined by a relatively simple combination of the electrical resistivity of the seafloor, the depth of the ocean, and the distance from the coastline. Because coast effect distortions operate over a variety of length scales related to the skin-length of the electromagnetic fields, care needs to be taken in the interpretation of seafloor MT data so that 2D and 3D distortions are properly accounted for. By including coastlines and bathymetry in 2D inversion and limiting the analysis to shorter period data that are less sensitive to 3D coast effect distortion, our broadband data constrained the thickness of conductive forearc sediments and the underlying high resistivity associated with the mantle wedge and subducting oceanic lithosphere.

Acknowledgments

K. Key and S. Constable acknowledge funding support from the Seafloor Electromagnetic Methods Consortium at Scripps Institution of Oceanography. We thank Lisl Lewis, Kazunobu Yamane, Arnold Orange, Jacques Lemire, Ed Nichols, Robert Mallan, GERD, JAMSTEC and the Captain and crew of the R/V Kaiyo for assistance carrying out the field work. Gary Egbert and Phil Wannamaker are thanked for making their processing and modeling algorithms publicly available. Two anonymous reviewers provided helpful suggestions for clarifying this work.

References

Alekseev, D.A., Palshin, N.A., Varentsov, I.M., 2009. Magnetotelluric dispersion relations in a two-dimensional model of the coastal effect. Izv-Phys. Solid Earth 45 (2), 167–170.
Baba, K., Chave, A.D., 2005. Correction of seafloor magnetotelluric data for topographic effects during inversion. J. Geophys. Res. 110, B12105, doi:10.1029/2004JB003463.
Baba, K., Seama, N., 2002. New technique for the incorporation of seafloor topography in electromagnetic modelling. Geophys. J. Int. 150 (2), 392–420.
Berdichevsky, M., Dmitriev, V.I., 2008. Models and Methods of Magnetotellurics. Springer, Berlin.
Berdichevsky, M.N., Zhdanov, M.S., 1984. Advanced Theory of Deep Geomagnetic Sounding. Elsevier, Amsterdam.
Booker, J.R., Favetto, A., Pomposiello, M.C., 2004. Low electrical resistivity associated with plunging of the Nazca flat slab beneath Argentina. Nature 429, 399–403.
Brasse, H., Eydam, D., 2008. Electrical conductivity beneath the Bolivian orocline and its relation to subduction processes at the South American continental margin. J. Geophys. Res. 113 (B7), B07109.
Caldwell, T., Bibby, H., Brown, C., 2004. The magnetotelluric phase tensor. Geophys. J. Int. 158 (2), 457–469.
Chave, A.D., Constable, S.C., Edwards, R.N., 1991. Electrical Exploration Methods for the Seafloor, pp. 931–969.
Constable, S., Heinson, G., 1993. In defence of a resistive oceanic upper mantle: reply to a comment by Tarits, Chave and Schultz. Geophys. J. Int. 114, 717–723.
Constable, S.C., Orange, A.S., Hoversten, G.M., Morrison, H.F., 1998. Marine magnetotellurics for petroleum exploration part I: a sea-floor equipment system. Geophysics 63 (03), 816–825.
Constable, S., Key, K., Lewis, L., 2009. Mapping offshore sedimentary structure using electromagnetic methods and terrain effects in marine magnetotelluric data. Geophys. J. Int. 176 (2), 431–442.
Cox, C., 1980. Electromagnetic induction in the oceans and inferences on the constitution of the earth. Geophys. Surv. 4, 137–156.
de Lugao, P.P., Wannamaker, P., 1996. Calculating the two-dimensional magnetotelluric Jacobian in finite elements using reciprocity. Geophys. J. Int. 127, 806–810.
deGroot Hedlin, C., Constable, S., 1990. Occam's inversion to generate smooth two-dimensional models from magnetotelluric data. Geophysics 55 (12), 1613–1624.
Egbert, G.D., 1997. Robust multiple-station magnetotelluric data processing. Geophys. J. Int. 130, 475–496.
Egbert, G.D., 2002. Processing and interpretation of electromagnetic induction array data. Surv. Geophys. 23 (2–3), 207–249.
Egbert, G.D., Booker, J.R., 1989. Multivariate analysis of geomagnetic array data 1, the response space. J. Geophys. Res. 94, 14227–14247.
Ferguson, I., 1988. The Tasman project of seafloor magnetotelluric exploration. PhD thesis, Australia National University, http://www.escholarship.org/uc/item/4767k3dm.
Filloux, J.H., 1973. Techniques and instrumentation for study of natural electromagnetic induction at sea. Phys. Earth Planet. Inter. 7 (3), 323–338.
Franke, A., Börner, R.-U., Spitzer, K., 2007. Adaptive unstructured grid finite element simulation of two-dimensional magnetotelluric fields for arbitrary surface and seafloor topography. Geophys. J. Int. 171 (1), 71–86.
Fujie, G., Ito, A., Kodaira, S., Takahashi, N., Kaneda, Y., 2006. Confirming sharp bending of the Pacific plate in the northern Japan trench subduction zone by applying a traveltime mapping method. Phys. Earth Planet. Inter. 157 (1–2), 72–85.
Gamage, S.S.N., Umino, N., Hasegawa, A., Kirby, S.H., 2009. Offshore double-planed shallow seismic zone in the NE Japan forearc region revealed by sP depth phases recorded by regional networks. Geophys. J. Int. 178 (1), 195–214.
Hayakawa, T., Kasahara, J., Hino, R., Sato, T., Shinohara, M., Kamimura, A., Nishino, M., Sato, T., Kanazawa, T., 2002. Heterogeneous structure across the source regions of the 1968 Tokachi-Oki and the 1994 Sanriku-Haruka-Oki earthquakes at the Japan trench revealed by an ocean bottom seismic survey. Phys. Earth Planet. Inter. 132 (1–3), 89–104.
Heinson, G., Constable, S., 1992. The electrical conductivity of the oceanic upper mantle. Geophys. J. Int. 110, 159–179.
Heinson, G., Lilley, F., 1993. An application of thin-sheet electromagnetic modelling to the Tasman sea. Phys. Earth Planet. Inter. 81, 231–251.
Hino, R., Ito, S., Shiobara, H., Shimamura, H., Sato, T., Kanazawa, T., Kasahara, J., Hasegawa, A., 2000. Aftershock distribution of the 1994 Sanriku-Oki earthquake (M_w 7.7) revealed by ocean bottom seismographic observation. J. Geophys. Res. 105 (B9), 21697–21710.
Hino, R., Azuma, R., Ito, Y., Yamamoto, Y., Suzuki, K., Tsushima, H., Suzuki, S., Miyashita, M., Tomori, T., Arizono, M., Tange, G., 2009. Insight into complex rupturing of the immature bending normal fault in the outer slope of the Japan trench from aftershocks of the 2005 Sanriku earthquake ($M_w = 7.0$) located by ocean bottom seismometry. Geochem. Geophys. Geosyst. 10, Q07O18.
Ito, S., Hino, R., Matsumoto, S., Shiobara, H., Shimamura, H., Kanazawa, T., Sato, T., Kasahara, J., Hasegawa, A., 2000. Deep seismic structure of the seismogenic plate boundary in the off-Sanriku region, northeastern Japan. Tectonophysics 319 (4), 261–274.
Ito, A., Fujie, G., Tsuru, T., Kodaira, S., Nakanishi, A., Kaneda, Y., 2004. Fault plane geometry in the source region of the 1994 Sanriku-Oki earthquake. Earth Planet. Sci. Lett. 223 (1–2), 163–175.
Itoh, Y, Tsuru, T., 2006. A model of late Cenozoic transcurrent motion and deformation in the fore-arc of northeast Japan: constraints from geophysical studies. Phys. Earth Planet. Inter. 156 (1–2), 117–129.
Jödicke, H., Jording, A., Ferrari, L., Arzate, J., Mezger, K., Ruepke, L., 2006. Fluid release from the subducted Cocos plate and partial melting of the crust deduced from magnetotelluric studies in southern Mexico: implications for the generation of volcanism and subduction dynamics. J. Geophys. Res. 111 (B8), B08102.
Jones, F., Price, A., 1970. The perturbations of alternating geomagnetic fields by conductivity anomalies. Geophys. J. R. Astr. Soc. 20, 317–334.
Kellett, R., Lilley, F., White, A., 1991. A 2-dimensional interpretation of the geomagnetic coast effect of southeast Australia, observed on land and sea-floor. Tectonophysics 192 (3–4), 367–382.
Key, K, Constable, S., 2002. Broadband marine MT exploration of the East Pacific Rise at 9°50′N. Geophys. Res. Lett. 29 (22), 11.1–11.4.
Key, K., Ovall, J. A parallel goal-oriented adaptive finite element method for 2.5D electromagnetic modeling, Geophys. J. Int., in revision.
Key, K., Weiss, C., 2006. Adaptive finite element modeling using unstructured grids: the 2D magnetotelluric example. Geophysics 71 (6), G291–G299.
Key, K.W., Constable, S.C., Weiss, C.J., 2006. Mapping 3D salt using the 2D marine magnetotelluric method: case study from Gemini prospect, Gulf of Mexico. Geophysics 71 (1), B17–B27.
Kurtz, R., DeLaurier, J., Gupta, J., 1986. A magnetotelluric sounding across Vancouver island detects the subducting Juan-de-Fuca plate. Nature 321 (6070), 596–599.
Li, Y., Key, K., 2007. 2D marine controlled-source electromagnetic modeling: part 1—an adaptive finite element algorithm. Geophysics 72 (2), WA51–WA62.
Li, Y., Pek, J., 2008. Adaptive finite element modelling of two-dimensional magnetotelluric fields in general anisotropic media. Geophys. J. Int. 175 (3), 942–954.
Li, S., Booker, J.R., Aprea, C., 2008. Inversion of magnetotelluric data in the presence of strong bathymetry/topography. Geophys. Prospect. 56 (2), 259–268.
Matsuno, T., Seama, N., Baba, K., 2007. A study on correction equations for the effect of seafloor topography on ocean bottom magnetotelluric data. Earth Planets Space 59 (8), 981–986.
Matsuno, T., Seama, N., Evans, R., Chave, A., Baba, K., White, A., Nori-Goto, T., Heinson, G., Boren, G., Yoneda, A., Utada, H., 2010. Upper mantle electrical resistivity structure beneath the central Mariana subduction system. Geochem. Geophys. Geosyst. 11 (9), Q09003.
Menvielle, M., Rossignol, J., Tarits, P., 1982. The coast effect in terms of deviated electric currents—a numerical study. Phys. Earth Planet. Inter. 28 (2), 118–128.
Mikada, H., Constable, S., Key, K., Uyeshima, M., Sayanagi, K., Fujie, G., KY00-02 Scientific Party, 2000. Marine magnetotellurics for the petrophysical identification of the seismogenic zone off Sanriku, Japan. Eos Trans. AGU 81 (48), Fall Meet. Suppl., Abstract S12D-05.
Nolasco, R., Tarits, P., Filloux, J.H., Chave, A.D., 1998. Magnetotelluric imaging of the Society Islands hotspot. J. Geophys. Res. 103 (B12), 30287–30309.
Parkinson, W., 1959. Directions of rapid geomagnetic fluctuations. Geophys. J. R. Astr. Soc. 2 (1), 1–14.
Parkinson, W., 1962. The influence of continents and oceans on geomagnetic variations. Geophys. J. R. Astr. Soc. 6 (4), 441–449.
Parkinson, W., Jones, F., 1979. The geomagnetic coast effect. Rev. Geophys. 17 (8), 1999–2015.

Rikitake, T., 1959. Anomaly of geomagnetic variations in Japan. Geophys. J. R. Astr. Soc. 2 (4), 276–287.
Schwarz, G., Krüger, D., 1997. Resistivity cross section through the southern central Andes as inferred from magnetotelluric and geomagnetic deep soundings. J. Geophys. Res. 102 (B6), 11957–11978.
Seama, N., Baba, K., Utada, H., Toh, H., Tada, N., Ichiki, M., Matsuno, T., 2007. 1-D electrical conductivity structure beneath the Philippine Sea: results from an ocean bottom magnetotelluric survey. Phys. Earth Planet. Inter. 162 (1–2), 2–12.
Stratton, J.A., 1941. Electromagnetic Theory. McGraw-Hill, New York.
Swift, C.M.J., 1986. A magnetotelluric investigation of an electrical conductivity anomaly in the southwestern United States. PhD Thesis, Massachusetts Institute of Technology, http://dspace.mit.edu/handle/1721.1/38346.
Tarits, P., Chave, A.D., Schultz, A., 1993. Comment on 'the electrical conductivity of the oceanic upper mantle' by G. Heinson and S. Constable. Geophys. J. Int. 114 (3), 711–716.
Tsuru, T., Park, J., Takahashi, N., Kodaira, S., Kido, Y., Kaneda, Y., Kono, Y., 2000. Tectonic features of the Japan trench convergent margin off Sanriku, northeastern Japan, revealed by multichannel seismic reflection data. J. Geophys. Res. 105 (B7), 16403–16413.
Wannamaker, P.E., Stodt, J.A., Rijo, L., 1987. A stable finite-element solution for two-dimensional magnetotelluric modeling. Geophys. J. R. Astr. Soc. 88, 277–296.
Wannamaker, P., Booker, J., Jones, A., Chave, A.D., Filloux, J.H., Waff, H., Law, L., 1989. Resistivity cross section through the Juan de Fuca subduction system and its tectonic implications. J. Geophys. Res. 94 (B10), 14127–14144.
Wannamaker, P.E., Caldwell, T.G., Jiracek, G.R., Maris, V., Hill, G.J., Ogawa, Y., Bibby, H.M., Bennie, S.L., Heise, W., 2009. Fluid and deformation regime of an advancing subduction system at Marlborough, New Zealand. Nature 460, 733–737.
White, S.N., Chave, A.D., Filloux, J.H., 1997. A look at galvanic distortion in the Tasman sea and the Juan de Fuca plate. J. Geomagnet. Geoelectr. 49 (11–12), 1373–1386.
Wight, D., Bostick, F., 1980. Cascade decimation—a technique for real time estimation of power spectra. In: Proceedings of the IEEE International Conference on Accoustic, Speech Signal Processing , pp. 626–629.